

Diffraction imaging of the Eagle Ford shale

I. Sturzu¹, A.M. Popovici¹, M.A. Pelissier², J.M. Wolak³ and T.J. Moser^{4*}

Abstract

Diffraction imaging is a novel technology that uses diffractions to image very small subsurface elements. Diffraction imaging may: (1) improve prospect characterization and pre-drill assessment of the local geology; (2) improve production and recovery efficiency; (3) reduce field development cost; and (4) decrease environmental impact. Field development may be accomplished with fewer wells to optimally produce the reservoir using high-resolution images of small-scale fractures in shale or carbonate intervals. Standard approaches to obtain high-resolution information, such as coherency analysis and structure-oriented filters, derive attributes from stacked, migrated images. Diffraction imaging, in comparison, acts on the pre-stack data, and has the potential to focus super-resolution structural information. Diffraction images can be used as a complement to the structural images produced by conventional reflection imaging techniques, by emphasizing small-scale structural elements that are difficult to interpret on a conventional depth image. An efficient way to obtain diffraction images is to first separate the migration events according to the value of the specular angle, in a similar way to offset gathers, and subsequent post-stack processing. The high-resolution potential is demonstrated by the diffraction images from the Kenedy 3D survey over the Eagle Ford shale, which show much more detail than conventional depth migration or coherence.

Introduction

In 2000 shale gas represented just 1% of American natural gas supplies. Today, it is 30% and the percentage keeps increasing. The technology to drill and fracture shale formations is now exported from the US to the rest of the world, increasing national oil and gas reserves in many other countries. Currently, there is a high level of activity for both shale gas and liquids production. Productivity in the shale plays depends on many factors including total organic content, the susceptibility of the reservoir to hydraulic fracturing and factors in the well design and completion processes. However, since fracture porosity plays a critical role, the detection of naturally occurring faults and fractures and the interaction of these with the hydraulic fracturing process are key areas of investigation. New high-resolution technologies are now used to visualize the structure and the natural fracture distribution and orientation in thin shale layers. Diffraction imaging is a new approach to image with super-resolution faults, pinch-outs, salt flanks, reflector unconformities, any small scattering objects, and is used as a complement to the structural image produced by reflection imaging. By identifying the areas with increased natural fracture density, reservoir engineers can design an optimal well placement programme that targets sweet spots, areas with increased

production, and minimizes the number of wells used for a prospective area.

Most detection methods are based on the use of conventional reflection seismic data (curvature, coherency, etc.). However, diffraction imaging offers the potential of higher resolution and reliability, as it is a direct method for the detection of subsurface discontinuities. The diffraction image is the direct response to subsurface discontinuities and is in most cases obtained from pre-stack, pre-migration data rather than post-stack, post-migration images. Using diffraction imaging we can obtain high-resolution 3D volumes of discontinuities in the earth such as small-scale faults, pinch-outs, salt flanks, reflector unconformities, in general small scattering objects. The diffractions volume can be used as a complement to the structural images produced by reflection imaging (Khaidukov et al., 2004; Taner et al., 2006; Moser and Howard, 2008; Koren et al., 2010; Dell and Gajewski, 2011; Moser, 2011).

In many of the shale resource areas the overburden is relatively straightforward. These conditions are ideal for focusing reflections, which also means that the diffraction imaging process is highly effective. In this paper, we make use of the recently developed workflow based on the role of specularity gathers (Sturzu et al., 2013), illustrating this on synthetic data and on a dataset from the Eagle Ford shale play of South Texas.

¹ Z-Terra, Inc.

² Roc Oil (Bohai) Company, formerly at Marathon Oil.

³ Tennessee Tech University, formerly at Marathon Oil.

⁴ Moser Geophysical Services.

* Corresponding author, E-mail: mosertj@gmail.com

Regional geology and seismic analysis of the Eagle Ford shale

The Eagle Ford shale, located in south-central Texas, is one of the most prolific regions for shale liquid production. Since 2008 more than 11,500 drilling permits have been issued, and as of November 2013, the Railroad Commission of Texas reported completion of 4690 oil wells in an area spanning 25 Texas counties. A wide range of fluids is present in the Eagle Ford play, including oil, wet gas, condensate and dry gas. As noted by previous workers, the heterogeneity of the play presents a number of exploration and production challenges (Treadgold et al., 2011; Royer and Peebles, 2012).

As shown in Figure 1, the Eagle Ford Shale overlies the Buda Limestone and is divided into two units: the Upper Eagle Ford and Lower Eagle Ford. An internal carbonate marker, the Kamp Ranch Member, separates the two and may be identified in wireline log signatures. In general, the lowermost Eagle Ford is characterized by high organic content (4-7% TOC) and moderate porosity (7-15%) (Treadgold et al., 2011). By contrast, the Upper Eagle Ford is significantly more calcareous and less organic rich (2-5% TOC). Total thickness of the Eagle Ford in south Texas ranges from 15 to 75 m. The upper and lower contacts are marked by unconformities with the Buda Limestone and Austin Chalk, respectively.

Rock properties vary significantly between the Buda, Eagle Ford and Austin Chalk, and regional 3D seismic analysis has proven effective for exploration (Yu et al., 2013; Treadgold et al., 2011). Predicting production, however, is more complex due to small-scale variations in organic content and pre-existing fracture networks. In general, previous workers have tried to characterize heterogeneity and fractures at two scales of observation. The 'large scale' approach makes use of reflection seismic for edge detection, using attributes such as curvature to define features in the Eagle Ford Formation. At the other end of the spectrum, 'fine scale' approaches attempt

to bring out sub-seismic fractures, e.g. measuring seismic anisotropy using equivalent medium theory.

Diffraction imaging

Diffractions are the seismic response of small elements (or diffractors) in the subsurface of the earth, such as small-scale faults, near-surface scattering objects and in general all objects which are small compared to the wavelength of seismic waves. Diffraction imaging is simply the process of using diffractions to determine the locations of the small subsurface elements that produced them. Since diffractors are, by definition, smaller than the wavelength of seismic waves, diffraction imaging provides super-resolution information, which consists of image details that are beyond the classical Rayleigh limit of half a seismic wavelength. The importance of diffractions in high-resolution structural imaging has been emphasized in many recent publications (Khaidukov et al., 2004; Taner et al., 2006; Moser and Howard, 2008; Koren et al., 2010; Dell and Gajewski, 2011; Moser, 2011). However, diffraction imaging is still not a widely used tool in seismic interpretation. In fact, most of the algorithms that are used to process seismic data enhance reflections and suppress diffracted energy. The goal of diffraction imaging is not to replace these traditional algorithms, but rather to provide interpreters with an additional image to fill in the small, but potentially crucial, structural and stratigraphic details.

The main goal of conventional time and depth seismic processing is to enhance specular reflections, which follow Snell's law and for which the angle of incidence equals the reflection angle. Many time processing steps are designed to increase the lateral coherency of the reflections – from interpolation, FXY deconvolution and FK filtering, to wave-equation binning. Since diffractions have a different move-out than reflections, many processing steps designed to enhance reflections result in attenuating diffractions. Seismic methods are generally limited

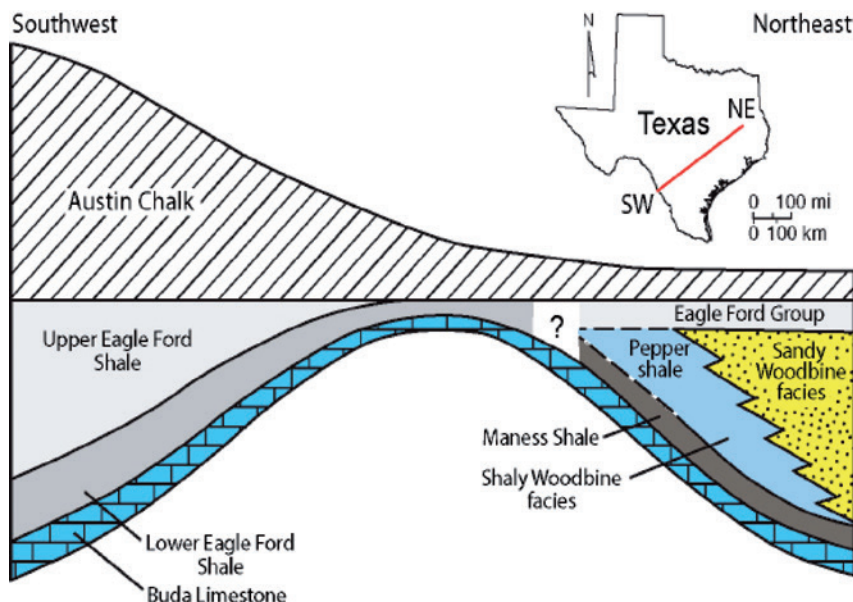


Figure 1 Cross section of Middle to Late Cretaceous rocks of south-central Texas. The Eagle Ford Formation pinches out to the northeast over the San Manco Arch. (After Hentz and Ruppel, 2010).

in their resolving power to about one half of the dominant wavelength at the target. When the sand or shale layers are thinner than half of the wavelength, tuning and multiple-reverberation effects make the stratigraphic interpretation of the images difficult and unreliable. Decreasing the wavelength of the seismic waves reflected at the target is nearly impossible in surface seismic surveying because of the dissipative nature of the overburden that causes the attenuation of the high-frequency component of the seismic wavefield. Furthermore, the high frequencies that are present in the data are often lost during standard processing.

An important point to note is that a true diffraction image is not optimally obtained by post-processing of a traditional seismic image, even if the seismic image is obtained by an algorithm that does not suppress diffractions. While diffractors will appear in the image, usually in the form of discontinuities, they have often much lower amplitudes than reflecting structures. By imaging diffractors using the pre-stack data, the diffractor amplitude can be enhanced while the specular reflections can be attenuated. Furthermore, discontinuities in the seismic image can appear for a variety of reasons other than diffractions, including small errors in the velocity model of the earth that was used to obtain the image.

Several techniques for diffraction imaging have been proposed (see references). They fall into two categories. In the first category are methods that separate the seismic data into two parts, one that contains the wave energy from reflections and the other that contains the wave energy from diffractions. Each component is used to provide an image through traditional seismic imaging methods. We have to keep in mind that there is no sharp distinction between reflected and diffracted waves (recall that by Huygens's principle, a reflector can be represented by a series of point diffractors that are positioned on its surface). In the second category are methods that do not separate the input seismic data, but rather use a different image-forming technique that suppresses reflecting surfaces in the image (Moser and Howard, 2008; Moser, 2009). We focus here on the second category of methods, specifically on the method of Moser and Howard, which can be expressed as a reflection suppressing kernel for Kirchhoff migration. In this approach, an accurate migration velocity model plays a central role and the focusing quality of the diffraction image is directly related to that of the standard migration image, with the same potential and the same limitations. If reflections can be focused, then they can also be suppressed, by using the same velocity model. The residual image is the diffraction image. The velocity sensitivity of the standard and diffraction image are therefore connected; we illustrate this below.

Specularity concept

A conventional Kirchhoff migration of the complete wave field forms a seismic image as a summation (stack) of the seismic events propagated to all possible locations in the subsurface ('complete wave' meaning reflections and diffractions

included). The propagation is done using travel-time tables computed in a given subsurface velocity model. The events propagated to locations which correspond to real reflections or diffractions within the subsurface, will be summed up coherently, while those propagated in locations where the velocity in the subsurface is not discontinuous will be averaged out. As for the former case, there is a quantitative difference between pure (specular) reflections and diffractions, a difference which comes from the fact that only for the specular events two close enough events will be propagated in two locations very close to each other. As a result, in the final stack, the specular events will have much higher amplitudes as compared to diffractive ones.

In the final image stack, a specular element can be approximated locally as a planar surface, with the isochron surface (computed from the exact travel-time tables) tangential to it. For diffractive events, there is no such constraint. As a measure of specularity for the image of a seismic event in a location from the subsurface, one can use the departure from Snell's law, quantified as the cosine of the angle formed by the gradient of the total travel time (computed from the source of the event to the image point and further to the receiver of the event), and the normal to the local planar surface defined in that image location. Specularity is then equal to unity for pure specular events following Snell's law and smaller for diffractions, the more they disagree with Snell's law.

Specularity gathers

The idea behind Kirchhoff diffraction imaging is to use a tapering procedure during the summation of the elementary seismic events, which will attenuate the events that are close to the specularity condition, while preserving the diffractive ones. The taper used for specularity suppression is obtained by the following steps. First, using *standard Kirchhoff migration* we obtain the seismic image. This image will include both reflections and diffractions, but as mentioned before, the reflections are the most dominant part of the image. The second step is *dip extraction*: to analyse the structures in the Kirchhoff image and determine the reflector normal vector to these structures at each image point. As for a specular reflection, this direction is collinear with the total travel time gradient; the taper function for those events will be zero. At a diffraction point, since the seismic waves propagate in all directions, the taper function will not be zero, at least for most of the wave propagation directions. The third step is the *diffraction imaging* proper, consisting of Kirchhoff migration using a well-calibrated specularity taper function.

The design of an effective specularity taper can be a challenge when done a priori (before migration), as the limits of pure specularity may vary as a function of subsurface location and orientation with respect to the data acquisition; they actually depend on the local size of the Fresnel zone which is difficult to estimate a priori. A simple trial-and-error method is computationally expensive since it requires repeated migrations and moreover is not likely to result in an optimal

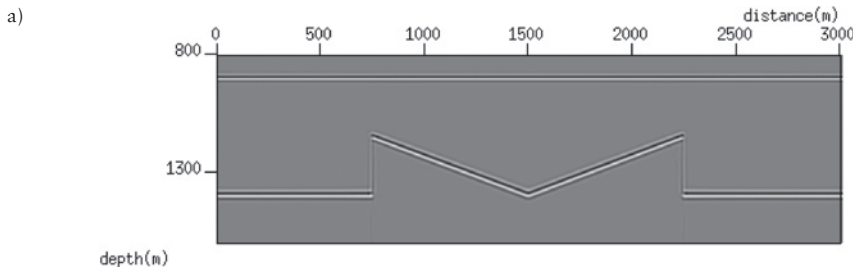


Figure 2 (a) Standard migration image over test model.

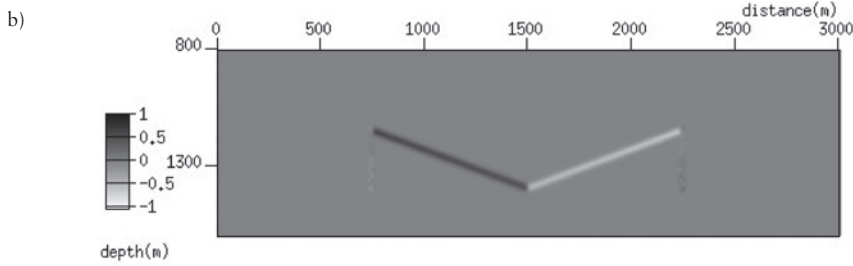


Figure 2 (b) Dip extraction from standard migration image (top/bottom: x/z component of reflector normal).

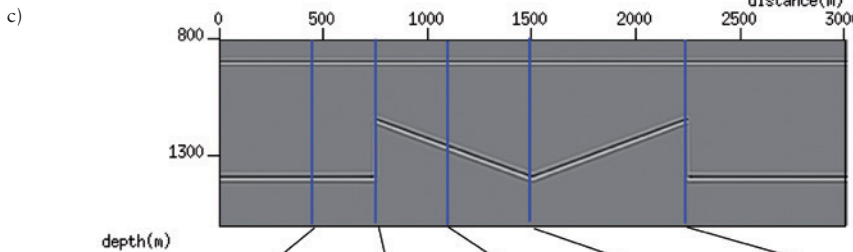
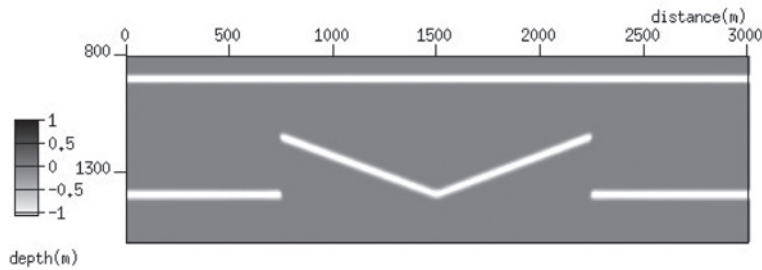


Figure 2 (c) Specularity gathers at horizontal locations denoted by the blue lines. Note that reflections result in energy concentrated at specularity equal to 1, but diffractions have specularity in the full range 0-1.

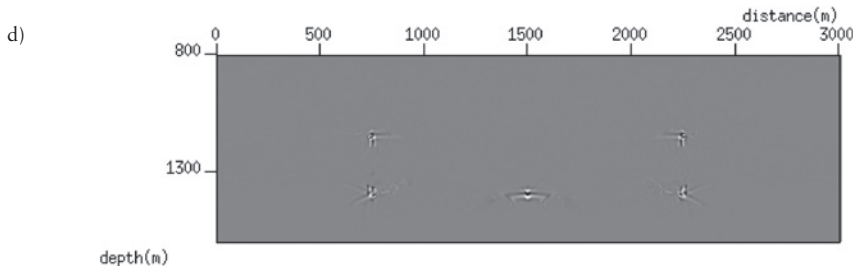
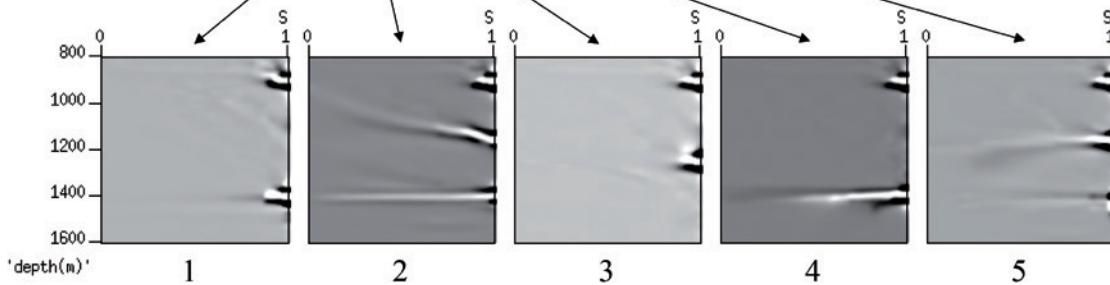


Figure 2 (d) Diffraction image over test model. Based on the specularity analysis of Figure 2c, reflection energy with specularity higher than 0.66 is suppressed.

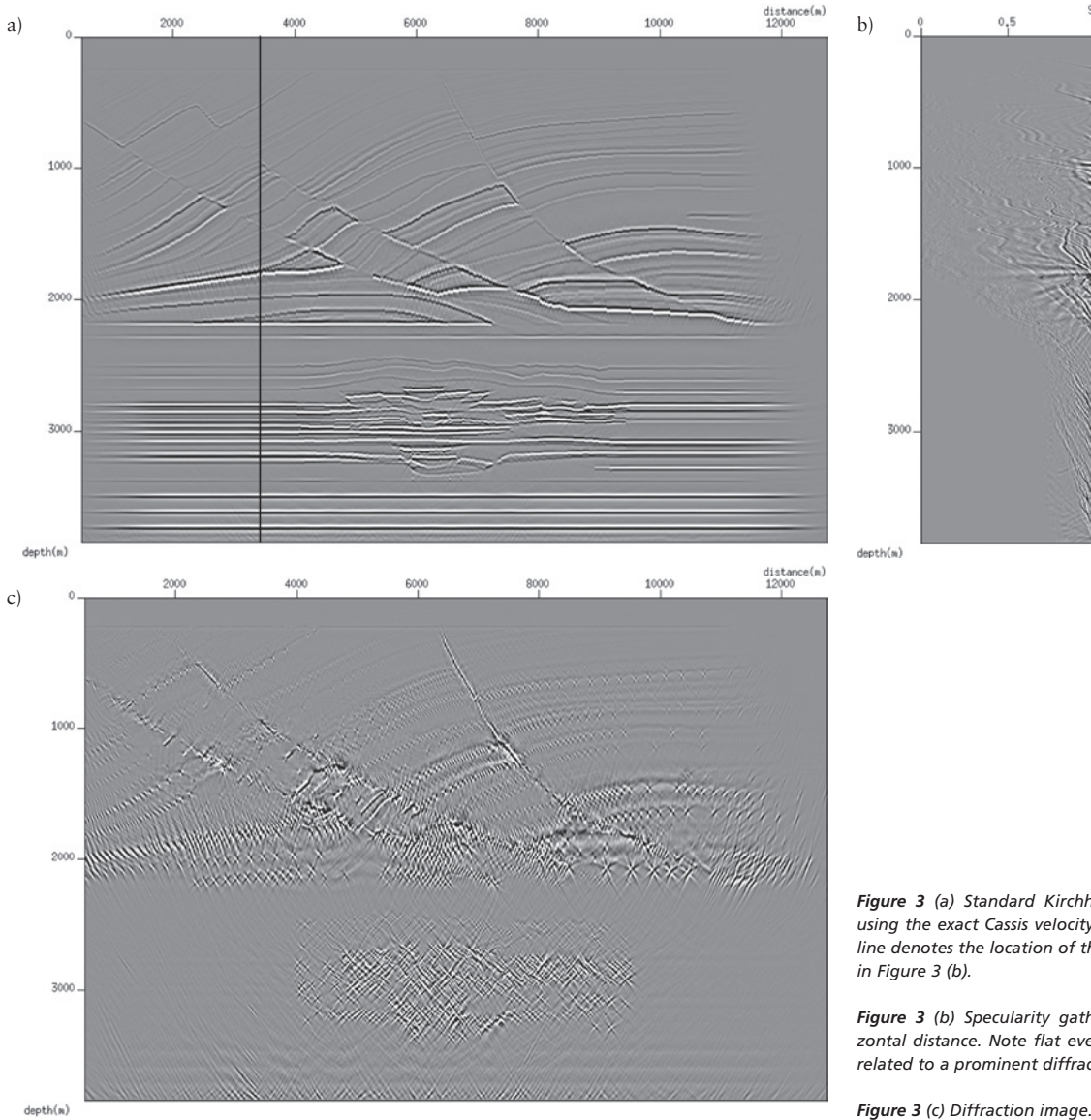


Figure 3 (a) Standard Kirchhoff migration stack using the exact Cassis velocity model. The vertical line denotes the location of the specularity gather in Figure 3 (b).

Figure 3 (b) Specularity gather at 3477 m horizontal distance. Note flat event at 1800 m depth related to a prominent diffraction.

Figure 3 (c) Diffraction image.

taper and diffraction image. The technique of *specularity gathers*, introduced by Sturzu et al. (2013), offers a solution and can be used to increase both the efficiency and accuracy of the diffraction imaging technique. During the migration, partial migration output is sorted with respect to specularity and stored in gathers which depend on specularity. After migration, the specularity taper can be efficiently designed by a small number of tests, the specularity gathers tapered and stacked over the specularity axis, resulting in an optimal diffraction image. This is a procedure which is very similar to the familiar process of sorting partial migration output in common-image gathers, depending on offset or reflection angle, and designing a mute function to properly mute unwanted (far-offset) energy (see Sturzu et al. (2013), for details).

The simple model of Figure 2 illustrates the workflow of diffraction imaging using specularity gathers. Figure 2a shows the standard migration in an exactly known velocity model, Figure 2b the result of dip extraction over the

standard migration image. Using this dip information, the specularity gathers are constructed, as shown at five typical locations in Figure 2c. Reflections are concentrated at focused spots for specularity equal to 1.0 (panels labelled 1 and 3), the other gathers show energy smeared out along flat events for a full specularity range of 0.0-1.0, associated with diffractions. After a small number of tests (in *post-migration* domain) we selected 0.66 as the optimal specularity cut-off for this case (other selections were applied for the other figures in the paper). The stack over the specularity tapered at this cut-off results in the diffraction image of Figure 2d. Here, reflections are fully suppressed and the diffracting edges are preserved and stand out. The Kirchhoff migrations shown in this paper were performed using a standard prestack depth migration programme, in which the diffraction imaging method was implemented in a special migration kernel and the dip field obtained using the plane wave destruction method.

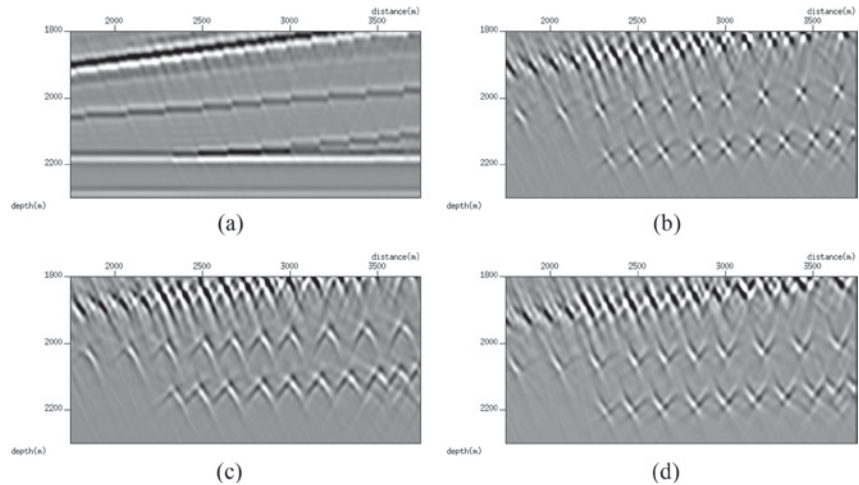


Figure 4 Details on a pinch-out from the Cassis model. (a) Kirchhoff migration and (b) Diffraction imaging using the correct velocity model (c) Diffraction imaging using a velocity lower with 1%. (d) Diffraction imaging using a velocity model higher with 1%.

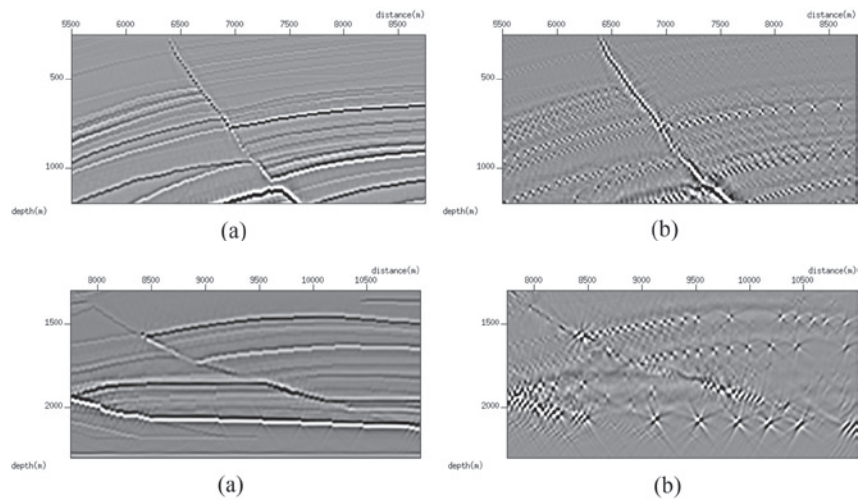


Figure 5 Details on a fault from the Cassis model. (a) Kirchhoff migration and (b) Diffraction imaging using the exact model.

Figure 6 Details on a rough horizon from the Cassis model. (a) Kirchhoff migration and (b) Diffraction imaging using the exact model.

A second example is the Cassis 2D seismic dataset developed at Total/Opera, Pau. The Cassis model has been previously investigated in Moser and Howard (2008) using a slant stack method for the dip field estimation. Figure 3 shows the complete-wave and the diffraction imaging Kirchhoff migration results. All the discontinuities visible in the full-wave stack (a) are enhanced in the diffraction image (c) while all the specular reflections are almost completely attenuated. In Figures 4-6 we show some details from Figures 3a and 3c. The details cover specific geological features able to produce diffractions: a pinch-out in Figure 4, a fault in Figure 5 and a rough horizon in Figure 6. In Figure 4, we compare the diffraction images computed using the exact velocity model and a velocity model change with -1% and 1% . One can clearly notice that most of the diffraction spots are well-focused in the exact model image, but they start showing the smile pattern even for a change as small as 1% in the velocity. This high sensitivity of the diffraction image transforms it into a valuable tool for velocity model building (a common theme in publications on diffraction imaging).

Eagle Ford shale

As a field example, we show here the application of the diffraction imaging workflow on the Kenedy 3D survey in the

south-western area of the Eagle Ford play. This survey area is characterized by a relatively uncomplicated velocity trend with mild lateral variations. As a result, there are no important challenges for the depth imaging, for instance, related to multi-pathing of energy. It therefore equally poses no important challenges to the diffraction imaging and qualifies as a very suitable area for its further deployment as a technology, and a step towards more complicated structural geometries.

Processing sequence

The diffraction imaging was conducted in the context of pre-stack depth migration of the complete wave field, preceded by pre-processing and pre-stack time migration. Particular attention points for a successful diffraction imaging included: pre-processing with special care to preserve high-frequency diffraction content and in the depth migration to arrive at an optimal velocity model, allowing optimal focusing of the standard migration image. This process consisted of several tomography iterations. When the velocity model was considered optimal, the resulting standard migration image was used for reflector dip extraction (using a plane wave destructor filter (Taner et al., 2006)). The reflector dip field and the travel-time tables of the final velocity iteration were

then used for the diffraction imaging. Specularity gather analysis (as described above) allowed us to efficiently select the best taper parameters to arrive at a high-quality diffraction image.

Switching off reflectivity – comparison of reflection and diffraction images

A typical output of the diffraction imaging is shown in Figure 7. Various degrees of specularity tapering show how

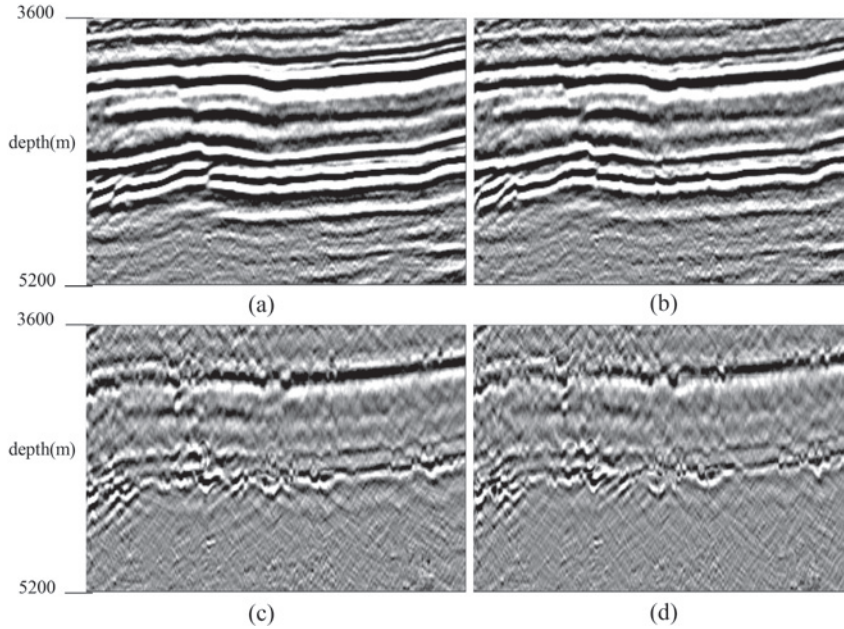


Figure 7 Switching off reflectivity: images over Eagle Ford. (a) standard depth image; (b) with weak tapering of specular reflectivity; (c) with increased tapering; (d) with optimal tapering = diffraction image.

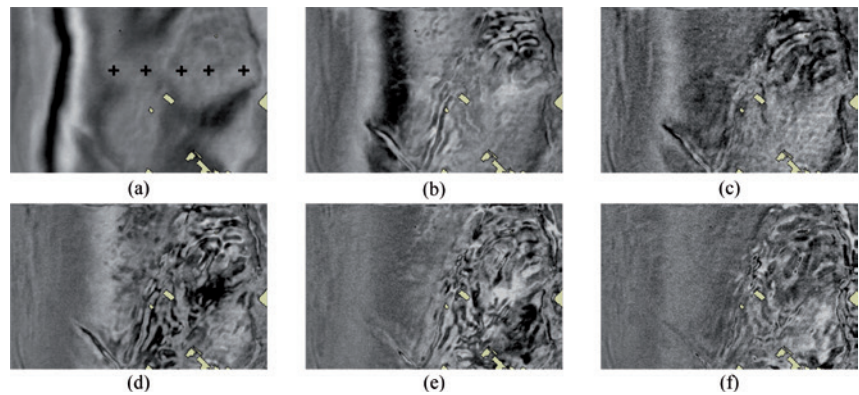


Figure 8 Depth slice zooms over Eagle Ford at depth 4790 m. (a) standard depth migration ('+' denote locations of specularity gathers shown in Figure 9), (b-f) diffraction images with increasing specularity suppression (cut-outs have not been part of the survey).

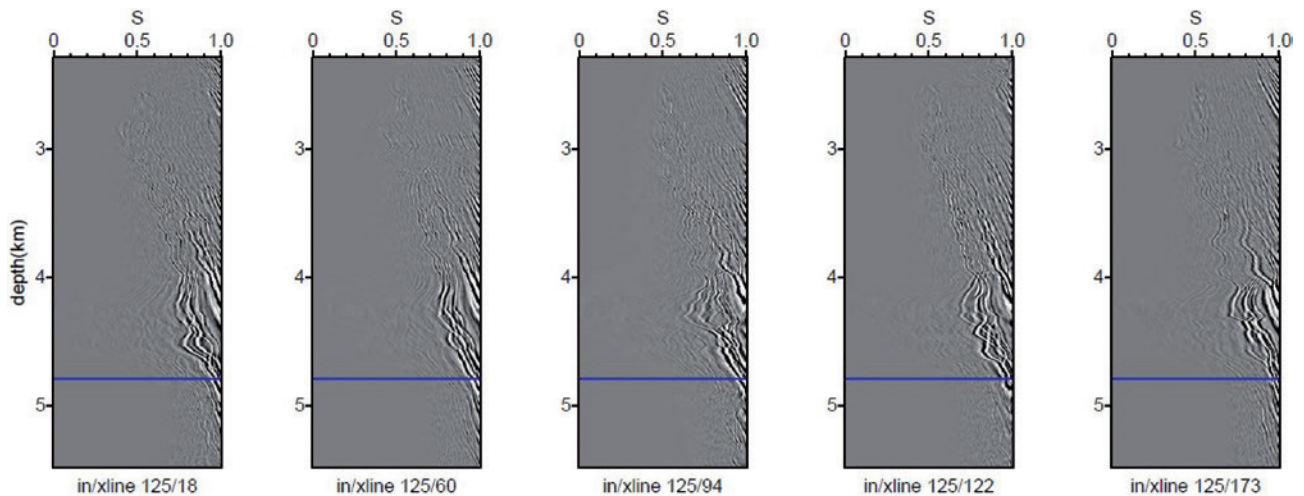


Figure 9 Specularity gathers at locations denoted '+' in Figure 8a, depth indicated by blue line.

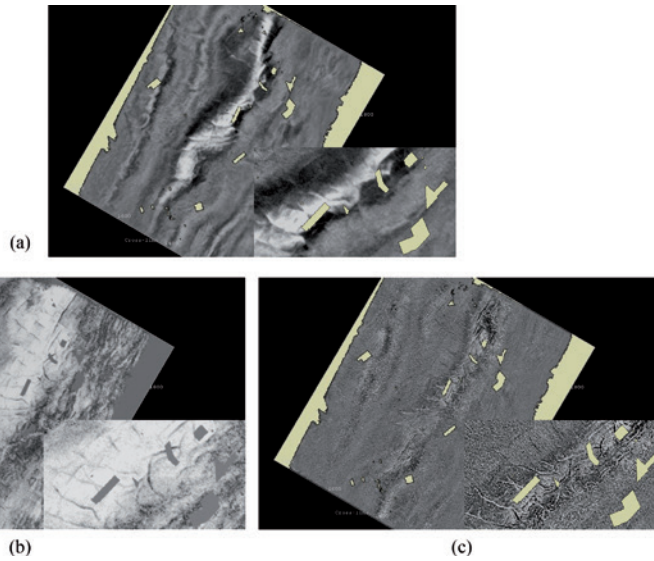


Figure 10 Depth slices over Eagle Ford at 2740 m. (a) standard depth migration, (b) coherence, (c) diffraction image.

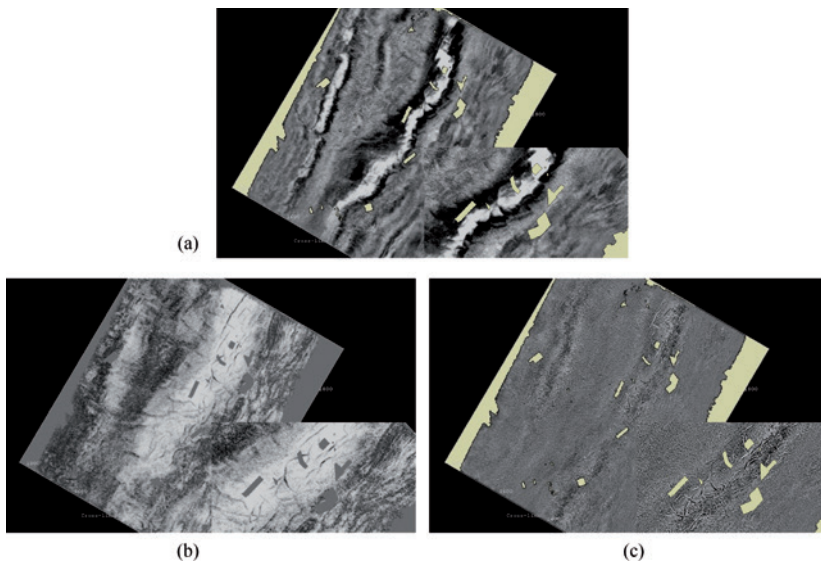


Figure 11 Depth slices over Eagle Ford at 2790 m. (a) standard depth migration, (b) coherence, (c) diffraction image.

the reflection content is gradually removed from the depth image (Figure 7a-d). At the same time, diffractivity in the form of diffraction images appears (diffractivity meaning the image after reflectivity is suppressed). The gradual disappearance of reflectivity clearly points to the fact that there is no sharp distinction between reflections and diffractions, but rather a smooth and frequency-dependent transition between the two. Diffractions compensate for discontinuities in the reflection wave field, thus ensuring continuity of the overall wave field (Klem-Musatov and Aizenberg, 1984). Residual reflectivity appears to be uplifted after specular suppression. This can be explained in terms of Fermat's shortest path principle: after removing specular reflections, ray paths in the vicinity of the specular reflection survive, but with a longer reflection time. Diffractions in comparison remain always at the same location.

It takes some practice to interpret the diffraction sections, but on closer inspection and in comparison with the corresponding standard migration image, (Figure 7a) the diffraction events

can be explained and serve as high-resolution complement of the complete wave events. Most diffraction events (Figure 7b-d) can be traced back to events weakly visible in the complete wave image, but are overshadowed by reflectivity on this image.

Figure 8 shows the effect of specular suppression of various degrees on depth slices for the Eagle Ford/Kenedy 3D survey, based on specularity gathers as displayed in Figure 9. From Figure 8a to 8f it becomes clear that an increasing tapering of specular reflection is accompanied by an increasing degree of diffraction detail (until an optimum is reached beyond which diffraction information is attenuated as well). As the tapering can be spatially variable and efficiently calibrated over the area of interest, the specularity gather analysis proves to be a valuable tool to select optimal taper parameters, in close coordination with the interpreter. We believe that this is a key advance and opens new capabilities in seismic interpretation.

The depth slices (Figure 10 to Figure 13) compare the diffraction image with both the standard depth migration image

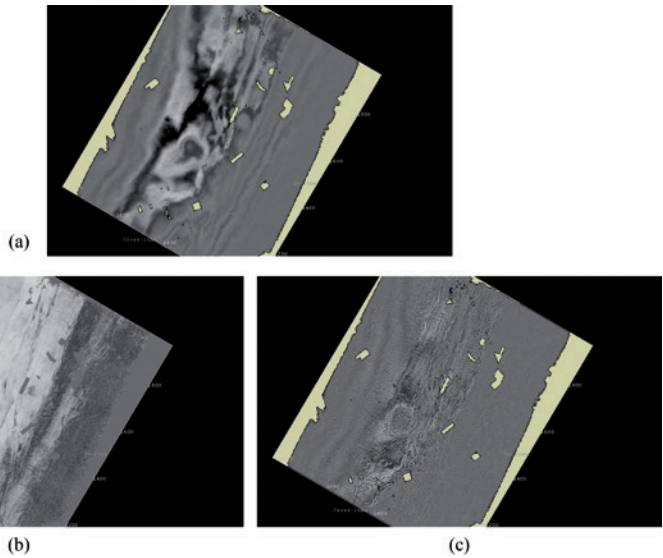


Figure 12 Depth slices over Eagle Ford at 4115 m. (a) standard depth migration, (b) coherence, (c) diffraction image.

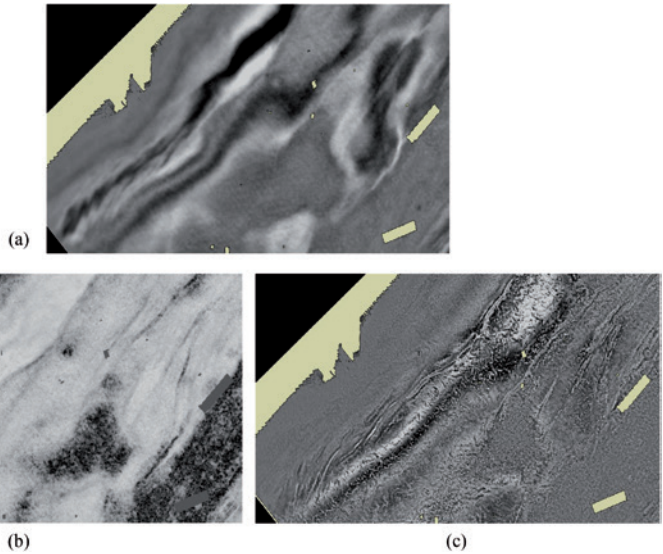


Figure 13 Depth slices over Eagle Ford at 4620 m. (a) standard depth migration, (b) coherence, (c) diffraction image.

and a coherence cube, extracted from the depth image. Here, coherence seems to have more detail for fault definition in some parts of the shallow slices. However, for the deeper slices the diffraction images consistently show much more detail. The section and depth slice zooms of Figure 13 confirm this. Even the zoom at the shallow depth of 2740 m (Figure 10) shows a much richer fault pattern of the diffraction image slice than on the coherence slice. A comparison of maximum curvature with the diffraction image shows similarly much more detail in the diffraction image (Figure 14).

Response of large scale faults

A typical seismic section is shown in Figure 15. Here we can observe the high reflectivity package which includes the Eagle Ford, the overlying Austin Chalk and the underlying Buda limestone. The overburden, although faulted, is not highly structured. Let us examine the seismic diffraction response of a major fault and compare this to the seismic

reflection response. Here, we begin with a migrated depth image of a line which runs approximately along the strike of the fault plane (Figure 16a). On this line we see little indication of the fault, except for a small area of disturbance. When we superimpose the diffraction image (Figure 16b) we notice that a strong diffraction response occurs not only at the discontinuity but also in areas where there is no apparent discontinuity in the reflection response. In Figure 16c we display the same crossline intersected with an inline. We observe a diffraction response on both the crossline and the inline. Now if we look only at the inline Figure 16d, we observe that the diffraction response is much more limited in extent. As shown in the reflection response (Figure 16e), it is clear that the diffraction response is due to a normal fault. The extended linear diffraction response seen on the crossline is the local response along the strike of the fault plane. On the reflection seismic image alone the presence of a fault strike plane is not obvious. However, the 3D diffraction image

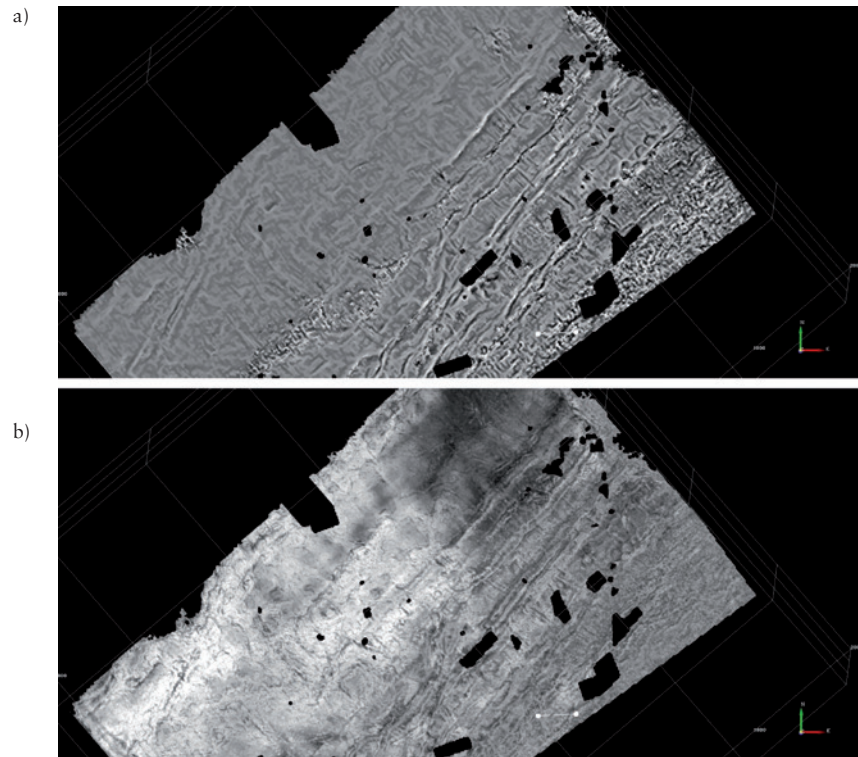


Figure 14 Depth slices over Eagle Ford at Top Buda (4570 m). (a) maximum curvature, (b) diffraction image.

makes no distinction between dip and strike. The superposition of the reflection and diffraction responses therefore provides a powerful interpretation tool.

Small-scale faulting

We now examine the spatial distribution of the diffraction response relative to the major faults. In Figure 17 we show a seismic cross section with the diffraction overlay along with a diffraction horizon slice. We can note that the diffractivity tends to be organized in north-east south-west trending bands running parallel to the major fault trends. We interpret the area of high diffractivity to be small-scale faults or fractures antithetic to the major faults. These features occur at the seismic scale but are too small to be observed on the conventional reflection seismic. Moreover, the dense diffraction distribution could be associated with an even finer scale of faulting and fracturing not detectable via the seismic method, beyond the resolution of surface seismic data.

Conclusions and future work

We used the reflector dip field extracted from a full-wave pre-stack Kirchhoff migration image to modify the tapering function of the migration kernel. As a result we enhanced the diffraction component of the image, while almost completely attenuating the specular reflections. We showed that the method is highly sensitive to changes in the velocity model, making it appropriate for velocity model building.

We recommend a comprehensive integration of the diffraction data with the production statistics to determine the level of correlation with previous and ongoing production.

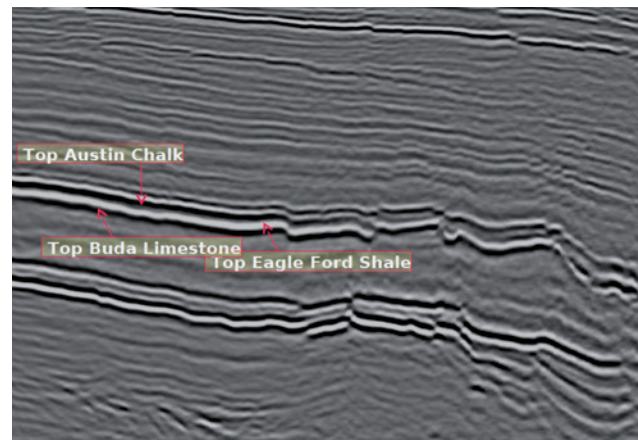


Figure 15 Eagle Ford Horizons on standard pre-stack depth migration image.

The diffractivity data can be treated as a seismic attribute with the understanding that the attribute is itself an intrinsic imaging product as opposed to the derivatives of the conventional reflection image.

Acknowledgements

We would like to thank Marathon Oil and Seitel for permission to show the Eagle Ford data, and Opera (Pau) for providing the Mare di Cassis data set. We also would like to thank the Marathon Upstream Technology and Eagle Ford Asset Teams for their support in this project and many useful discussions. All images in the paper were obtained using Z-Terra's Kirchhoff pre-stack depth migration software (ZTK), with adapted modules for diffraction imaging.

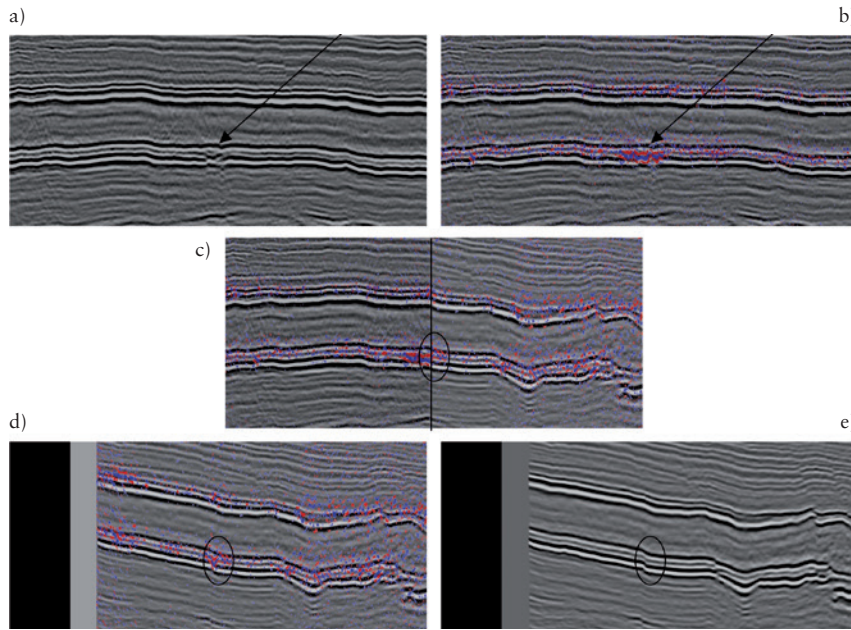
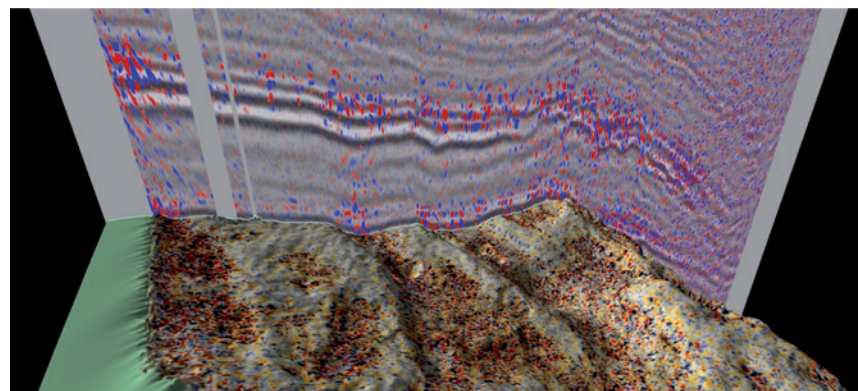


Figure 16 Response of large-scale faults – crossline section, running approximately along the strike of the fault plane. (a) Standard depth image. Note that there is little indication of the fault, except for a small area of disturbance. (b) With diffractivity superimposed in a purple colour scale. Note the strong diffractivity not only at the discontinuity but also in areas with no apparent discontinuity in reflectivity. (c) Diffractivity on both the crossline and the inline. (d) Inline section only. (e) Reflectivity only. Note that the diffractivity is much more limited in extent, indicating a normal fault.

Figure 17 Seismic cross-section with the diffraction overlay along with a diffraction horizon slice. Note that the diffractivity trends are organized in NE-SW trending bends running parallel to the major fault trends. These trends can be interpreted as small-scale faults or fractures antithetic to the major faults, but are too small to be observed on the standard reflection seismic image. The dense diffraction distribution could be associated with an even finer scale of faulting and fracturing not detectable via the seismic method, beyond the resolution of surface seismic data.



References

Dell, S. and Gajewski, D. [2011] Common-reflection-surface-based workflow for diffraction imaging. *Geophysics*, 76, 187-195.

Hentz, T.F. and Ruppel, C. [2010] Regional lithostratigraphy of the Eagle Ford Shale: Maverick Basin to East Texas Basin. *Gulf Coast Association of Geological Societies Transactions*, 60, 325-337.

Khaidukov, V., Landa, E. and Moser, T.J. [2004] Diffraction imaging by focusing-defocusing: An outlook on seismic super-resolution. *Geophysics*, 69, 1478-1490.

Klem-Musatov, K.D. and Aizenberg, A.M. [1984] The ray method and the theory of edge waves. *Geophys. J. R. Astr. Soc.*, 79, 35-50.

Koren, Z., Ravve, I. and Levy, R. [2010] Specular-diffraction Imaging by Directional Angle Decomposition. *72nd EAGE Conference Barcelona*, Extended Abstracts.

Moser, T.J. and Howard, C.B. [2008] Diffraction imaging in depth. *Geophysical Prospecting*, 56, 627-641.

Moser, T.J. [2011] Edge and Tip Diffraction Imaging in Three Dimensions. *73rd EAGE Conference Vienna*, Extended Abstracts.

Royer, T. and Peebles, R. [2012] Predicting productivity in the Eagle Ford through the integration of seismic, geologic and engineering attributes. *74th EAGE Conference Copenhagen*, Extended Abstracts.

Shtivelman, V. and Keydar, S. [2005] Imaging shallow subsurface inhomogeneities by 3D multipath diffraction summation. *First Break*, 23, 39-42.

Sturzu, I., Popovici, A.M., Tanushev, N., Musat, I., Pelissier, M.A. and Moser, T.J. [2013] Specularity Gathers for Diffraction Imaging. *75th EAGE Conference London*, Extended Abstracts.

Taner, M.T., Fomel, S. and Landa, E. [2006] Separation and imaging of seismic diffractions using plane wave decomposition. *76th SEG meeting New Orleans*, Expanded Abstracts.

Treadgold, G., Campbell, B., McLain, B., Sinclair, S. and Nicklin, D. [2011] Eagle Ford shale prospecting with 3D seismic data within a tectonic and depositional system framework. *The Leading Edge*, 30, 48-53.

Yu, J., van Gisbergen, S., Dwan, S.F., Yuan, R., Hackbarth, C., Shi, S., and Lambrecht, J. [2013] Technologies unlocking unconventional gas resources – Field case studies from North America and China. *2013 International Petroleum Technology Conference Beijing*, Expanded Abstracts.

Received: 19 February 2014; Accepted: 11 June 2014.
doi: 10.3997/1365-2397.2014016